# STABILITY ANALYSIS OF IMMOBILIZED OZONATED VEGETABLE OIL ON SILICA NANOPARTICLES

Nur Amira Rosdi[1], Aliff Rahimi Sha'ary[1], Yusilawati Ahmad Nor[1*],  Dzun Noraini Jimat[1], Kim Yeow Tshai[2]

[1]*Department of Chemical Engineering and Sustainability, Kulliyyah of Engineering, International Islamic University. Malaysia (IIUM), Jalan Gombak, 53100 Kuala Lumpur, Malaysia.*
[2]*Department of Mechanical, Manufacturing and Materials Engineering, Faculty of Science and Engineering, University of Nottingham Malaysia, Jalan Broga, 43500 Semenyih, Selangor, Malaysia*

*\*Corresponding author: yusilawati_ahmadnor@iium.edu.my*

***ABSTRACT:*** Ozonated vegetable oils (OVO) have therapeutic potential due to their antimicrobial, anti-inflammatory, and wound-healing properties. However, their wettability and stability in aqueous solutions remain challenging, hampering their bioavailability. Silica nanoparticles offer a promising solution for enhancing bioavailability and controlled release of various hydrophobic drugs, yet a similar approach has yet to be investigated with OVO. Thus, this study uses silica nanoparticles of ±100 nm as delivery vehicles to alter the wettability and stability of ozonated olive oil (OOO) in aqueous medium. The study includes preparing and characterizing non-porous and porous silica nanoparticles for OOO immobilization using rhamnolipid biosurfactants as a linker agent. Both non-porous and porous silica nanoparticles, synthesized via a modified Stöber method, were compared in terms of structure and ability to immobilize OOO for wettability improvement. TEM and XRD revealed structural characteristics of the synthesized silica nanoparticles, confirming the amorphous solid and porous structure of the nanoparticles with an average size measured below 100 nm for both nanoparticles. FTIR spectroscopy confirmed the successful immobilization of OOO on both silica nanoparticles showing the higher intensity of OOO on the non-porous silica nanoparticles (NPSiNPs) compared to porous silica nanoparticles (PSiNPs). DLS data shows that NPSiNPs had a mean size of 91.54 nm, while PSiNPs had a mean size of 201.5 nm, with both having low PDI values (<0.5). Incorporating OOO onto silica nanoparticles, with rhamnolipid, significantly improved wettability and prolonged stability of OOO, maintaining over 80% of the OOO-silica nanocomposite in the water suspension after 3 days for NPSiNPs and over 50% for PSiNPs. The study highlights the synergistic effects of biosurfactants and silica nanoparticles in enhancing the stability and bioavailability of OVO in aqueous medium, which could contribute to advancements in therapeutic applications.

***KEYWORDS:*** *Silica nanoparticles, Rhamnolipid, Wettability, Immobilization, and Ozonated olive oil.*

## 1. INTRODUCTION

Ozone, being highly reactive, readily interacts with unsaturated fatty acids present in triglycerides of vegetable oils, forming various oxygenated products like ozonides, peroxides, and aldehydes, following the mechanism explained by Criegee [1]. The interaction of ozone with vegetable oils to produce ozonated vegetable oil (OVO) offers benefits beyond antimicrobial and anti-inflammatory effects [2, 3], potentially stimulating

tissue regeneration and repair [1]. This suggests the potential implementation of OVO in the public health system as an antimicrobial additive in cosmetic and pharmaceutical products, primarily for topical application to treat wounds or skin diseases [4]. Ozonated olive oil (OOO) has been used specifically for skin treatment, therapeutic agents, orthopedics treatment, and organ movement traumatology [5]. However, due to its superhydrophobic and lipophilic nature [6], the biological efficacy of OOO is limited in aqueous environments [7, 8]. Researchers have used chemical surfactants like DMSO and Tween 80 to improve water solubility, but these agents are not eco-friendly and may be toxic to cells [9, 10]. In contrast, biosurfactants offer a more sustainable solution with lower toxicity and higher biodegradability. However, their use to enhance the wettability of OOO along with nanoparticles in aqueous solutions remains unexplored.

Silica nanoparticles have garnered significant attention in drug delivery research in recent years. Their unique properties, such as high surface area, biocompatibility, and ease of functionalization, make them ideal candidates for drug delivery systems [11]. Moreover, silica nanoparticles can be tailored into various morphologies, allowing for precise control over their size, surface charge, and other characteristics, which enhances their effectiveness as drug carriers. Additionally, their ability to incorporate a wide range of molecules, including hydrophobic drugs and essential oil with controlled release behavior, further improves their suitability in drug delivery applications [11, 12]. When biosurfactants are immobilized on silica nanoparticles, they stabilize the particles by preventing aggregation [9], enhancing dispersibility and functionality. This stabilization is crucial for applications requiring controlled release and improved bioavailability of bioactive compounds, making silica nanoparticles functionalized with biosurfactants a promising approach in modern drug delivery research [13].

The combination of biosurfactant-immobilized silica nanoparticles was reported to offer a synergistic effect, where the biosurfactant stabilizes the nanoparticles and alters the wettability properties of oil for easy recovery [14-15]. To date, the same approach has not been demonstrated for OVO to improve OVO wettability and stability in aqueous solution. Thus, in this study, biosurfactant (rhamnolipid) immobilized silica nanoparticles of the non-porous and porous structure were prepared as delivery vehicles for OOO, and the effect of nanoparticles structure on the wettability and stability of OOO in water were investigated. Possible mechanisms of OOO immobilization on the silica nanoparticles were described as in Fig. 1.

Fig. 1 (a) and (b) show biosurfactant behaves as the linker agent, which binds through physical interaction either on the surface or pores of silica nanoparticles. The amphiphilic properties of biosurfactants facilitate the immobilization of OVO on silica nanoparticles. The surface hydroxyl groups (Si-OH) on silica nanoparticles serve as active sites for biosurfactant binding. The hydrophilic heads of the biosurfactants interact with these silanol groups, while their hydrophobic tails form a hydrophobic layer that facilitates OVO attachment. The novel system is expected to improve the bioavailability of the OOO, making it a valuable approach for cosmetic and medical applications to maximize its therapeutic benefits while minimizing potential side effects.
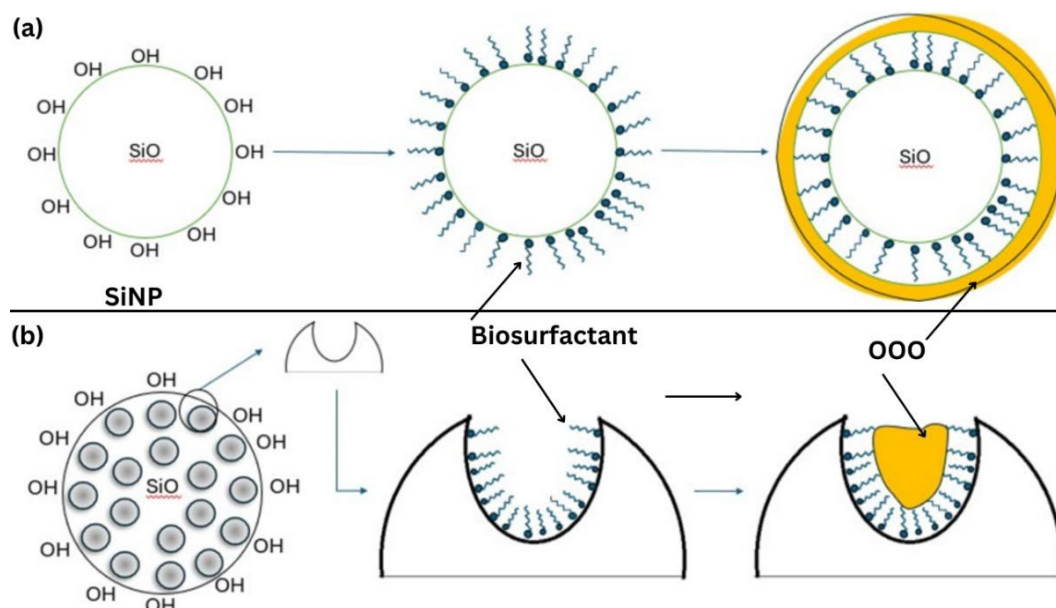
Fig. 1. Possible mechanism of OOO immobilization on (a) NPSiNPs and (b) PSiNPs.

## 2. MATERIALS AND METHODOLOGY

### 2.1. Chemical and Materials

Olive oil, 100% extra virgin olive oil (BestOlio), was obtained from a local market. An Absolute Ozone NANO ozone generator was used in the ozonation process. To synthesize the silica nanoparticles, tetraethyl orthosilicate (TEOS), ammonium hydroxide (NaOH), absolute ethanol (purity $\geq$ 99.8%), and Cetyltrimethylammonium Bromide (CTAB) were obtained from Chemiz and Sigma Aldrich.

### 2.2. Preparation of Non-porous Silica Nanoparticles

In synthesizing non-porous silica nanoparticles (NPSiNPs) in the range size of 100 nm, the common steps involve using modified Stöber methods [15]. Ethanol (29 ml) was mixed with 1.6 ml of deionized water and 3 ml of NaOH. After stirring thoroughly, 3 ml of TEOS was added, and the solution was stirred for 2 hrs. at a temperature of 70 °C. The solution obtained was centrifuged at 10,000 rpm for 50 mins. After centrifugation, the supernatant was discarded, and the pellet was washed twice with ethanol to remove surface-adsorbed reagents. The centrifuge tubes containing the pellet were then wrapped with perforated aluminum foil and placed in a drying oven at 50 °C overnight. The NPSiNPs were ground into a fine powder using a mortar and pestle. The sample was then kept in the tube for preservation.

### 2.3. Preparation of Porous Silica Nanoparticles

The synthesis of porous silica nanoparticles (PSiNPs) was adapted from the previous study [15]. The process began with 16 ml of a 25 wt% CTAB solution, and 0.08 ml of triethanolamine was added to 20 ml of deionized water. The mixture was gently stirred at 60°C for 1 hr. in a round-bottom flask. After thorough stirring, 1.5 ml of TEOS and 1 ml of cyclohexane were added, and the solution was stirred gently at the same temperature for an additional 6 hrs. The resulting solution was then centrifuged at 10,000 rpm for 60 minutes, and the pellet was washed twice with ethanol. The collected pellet of PsiNPs undergoes calcination by heating at 220 °C for 3 hrs. to remove the CTAB template [16]. After

calcination, the PSiNPs were ground into a fine powder using a mortar and pestle and stored in tubes.

## 2.4. Preparation of ozonated vegetable oils

To prepare ozonated olive oil (OOO), 20 ml of olive oil was ozonated in a Dresher bottle (Quickfit®) connected to an ozone generator. Ozone is produced by silent oxygen discharge (purity of 99.9%) from the ozone generator with 1 mg/l ozone concentration and adjustable ozone flow rate. The olive oil was exposed to the ozone gas at room temperature for 120 min with a 1.5 l/min ozone flow rate [17].

## 2.5. Incorporation of ozonated olive oil and biosurfactant on silica nanoparticles

With minor modifications, the preparation method for immobilizing biosurfactants on silica nanoparticles was adapted from a previous study [1]. To prepare the biosurfactant-modified silica nanoparticles (BS-SiNPs), 50 mg of NPSiNPs and PsiNPs were added to a biosurfactant solution with a concentration of 0.2% by weight. Rhamnolipid was selected as the biosurfactant for this study. To ensure uniform distribution of the nanoparticles, the SiNPs were stirred at room temperature for 2 hrs. and then ultrasonicated at 48 °C for an additional 2 hrs. The immobilization of OOO onto BS-SiNPs followed the method of the previous study [1]. For this, 50 mg of BS-SiNPs were mixed with 0.1 ml of OOO in a 2 ml centrifuge tube. The mixture was then left to react for 2 hrs.

## 2.6. Characterization of Silica Nanoparticles

### 2.6.1. Transmission Electron Microscopy (TEM)

TEM was utilized to confirm the presence of porous and non-porous structures and the synthesized nanoparticles' size and morphology. The samples were first dispersed using a water bath sonicator in an ethanol solution. A drop of the nanofluid suspension was then dispersed onto a carbon-coated copper grid, which was then left to dry at room temperature. The images were obtained using a TEM (CM 12, Philips) operated at an acceleration voltage of 120 kV.

### 2.6.2. X-Ray Diffraction Spectroscopy

X-ray diffraction (XRD) analysis was conducted to investigate the structural properties of silica nanoparticles and confirm their amorphous morphology. A powdered sample of the silica nanoparticles was carefully prepared and placed on a sample holder. The diffraction patterns were recorded using a Bruker D8 high-resolution X-ray diffractometer with CuK$\alpha$ radiation ($\lambda = 1.5406$ Å), operating at 40 kV and 30 mA. The scan range was set from 20° to 80° $2\theta$, with a step size of 0.02° and a scan rate of 1° per minute. The XRD patterns were then analyzed to determine the presence or absence of crystalline phases.

### 2.6.3. FT-IR Spectroscopy

FTIR spectroscopy was used to determine the chemical composition and the presence of OOO in the samples. The samples, prepared in powder form, were directly analyzed using the instrument. The FTIR spectra were recorded across a wavenumber range of 4000 - 400 cm$^{-1}$ with an Alpha ll Bruker spectrometer. The intensities of the absorption bands were measured as transmittance. The resulting spectra were then analyzed to identify the characteristic absorption bands associated with various functional groups in the samples.

### 2.6.4. Dynamic Light Scattering (DLS)

DLS measurements were conducted to determine the particle size distribution and polydispersibility index (PDI) of the samples. The samples were prepared by dispersing them in deionized water to achieve an appropriate concentration. Measurements were performed using a Malvern Zetasizer Panalytical. Data analysis provided the average particle size, the distribution profile, and PDI values.

## 2.7. Wettability and Stability test of immobilized ozonated olive oil

The samples were prepared by dispersing them in deionized water to achieve a 1 mg/ml concentration. UV-vis was measured by Lambda 950 UV-vis spectrophotometer in the spectral range of 400 nm. UV-visible light absorption measurements are applied to evaluate the stability of nanoparticles loaded with OOO.

# 3. RESULTS AND DISCUSSIONS

## 3.1. Characterization of Non-porous and Porous Silica Nanoparticles

TEM analysis has elucidated the morphology of both porous and non-porous silica nanoparticles. Fig. 2 (a) shows that NPSiNPs exhibit a consistent spherical shape with minimal aggregation and effective distribution throughout the grid. The average particle size of the NPSiNPs was around ±80 nm. In contrast, Fig. 2 (b) illustrates the TEM analysis of PSiNPs, which reveals a spherical morphology with porous structures. Despite the successful formation of porous features, TEM images reveal particle aggregation, which can be attributed to the porous nature of the nanoparticles. The high surface area of the porous silica nanoparticles enhances intermolecular forces between particles, promoting aggregation. Additionally, the rough surface morphology of the porous nanoparticles further increases their susceptibility to interactions, leading to particle clumping [9, 16].

The XRD patterns of both PSiNPs and NPSiNPs display a broad diffuse peak maximum observed at $2\theta = 21°$, which is a characteristic signature of amorphous silica material that lacks the long-range periodic order needed for sharp diffraction peaks [18]. The broad hump around $2\theta = 20°$ to $40°$ is a well-known signature of amorphous silica [19]. NPSiNPs exhibit a higher intensity, suggesting a more compact and dense structure than PSiNPs. This observation aligns with the principle that higher density results in stronger diffraction intensity. In contrast, the broader and lower-intensity peak in PSiNPs indicates greater structural disorder. The presence of porosity introduces voids that disrupt the regular atomic arrangement, leading to diminished constructive interference [18].

## 3.2. Immobilization of SiNPs with Ozonated Olive Oil

### 3.2.1. FTIR

FT-IR spectra shown in Fig. 3 confirm the immobilization of OOO and rhamnolipid biosurfactant (BS) on both NPSiNPs and PSiNPs. Both NPSiNPs and PsiNPs have the presence of distinct peaks around 1100 cm⁻¹ corresponding to asymmetric stretching vibrations of Si-O-Si and at approximately 800 cm⁻¹ and 400 cm⁻¹ correspond to the symmetric stretching vibrations of the Si-O functional groups, which confirms the characteristic of silica nanoparticles [12, 13].

For both BS-NPSiNPs and BS-PSiNPs, interactions result in the formation of Si–O–C bonds, which are observed around 1050 cm$^{-1}$. The hydrogen bonding and O–H stretching vibrations are diminished within the 3200–3600 cm$^{-1}$ range. The peak intensity decreases compared to BS alone, signifying successful immobilization of BS onto SiNPs. The spectra indicate that the immobilized BS retains its chemical functionality as in its free form. Compared to pure BS, the spectrum displays distinct peaks corresponding to O–H, C–H, C=O, and C–O–C groups. The hydroxyl (-OH) groups from the rhamnose component show broad stretching in the 3200–3600 cm$^{-1}$ region, indicating hydrogen bonding and water solubility. The C–H bonds in the lipid tail are observed at 2850–2960 cm$^{-1}$, contributing to hydrophobicity and interaction with nonpolar surfaces, which aids in surface tension reduction. The C=O stretching peak at 1730 cm$^{-1}$ is indicative of ester and carboxylic acid groups, while the ether bonds (C–O–C) present in glycosidic linkages show stretching vibrations in the 1050–1150 cm$^{-1}$ [20].
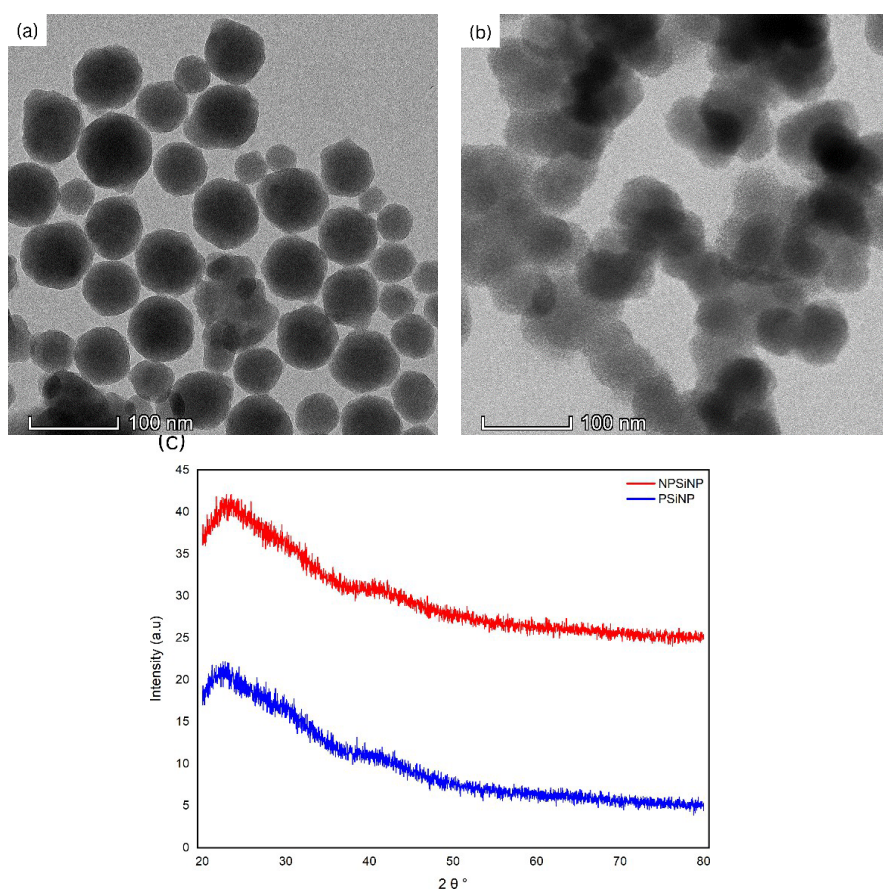


Fig. 2. TEM analysis results on (a) NPSiNPs, (b) PsiNPs, and (c) XRD patterns of silica nanoparticles.

The immobilization of OOO onto BS-SiNPs shows key differences between non-porous and porous structures. For OOO-BS-NPSiNPs, the O–H stretching band around 3200–3600 cm$^{-1}$ disappears, indicating a complete interaction with the surface, leaving no free hydroxyl groups. In contrast, for OOO-BS-PSiNPs, the O–H peak is still present but weakened, suggesting that while the interaction is strong, some hydroxyl groups remain exposed due to porosity. The C=O stretching at 1730 cm$^{-1}$ and Si–O–C bonds around 1050

cm$^{-1}$ confirm successful covalent bonding in both structures, while the hydrophobic C–H stretching at 2850–2960 cm$^{-1}$ indicates stabilization of the system [21]. The intensity of OOO in NPSiNPs is slightly higher compared to PSiNPs, possibly due to the aggregation behavior of PSiNPs observed in the TEM images, as shown in Fig. 2 (a) and (b). This aggregation could reduce the available surface area for OOO immobilization, leading to the observed difference in intensity. Hence, it is crucial to control and minimize aggregation to maintain the high surface area and reactivity of nanoparticles for effective drug delivery or other applications [22].
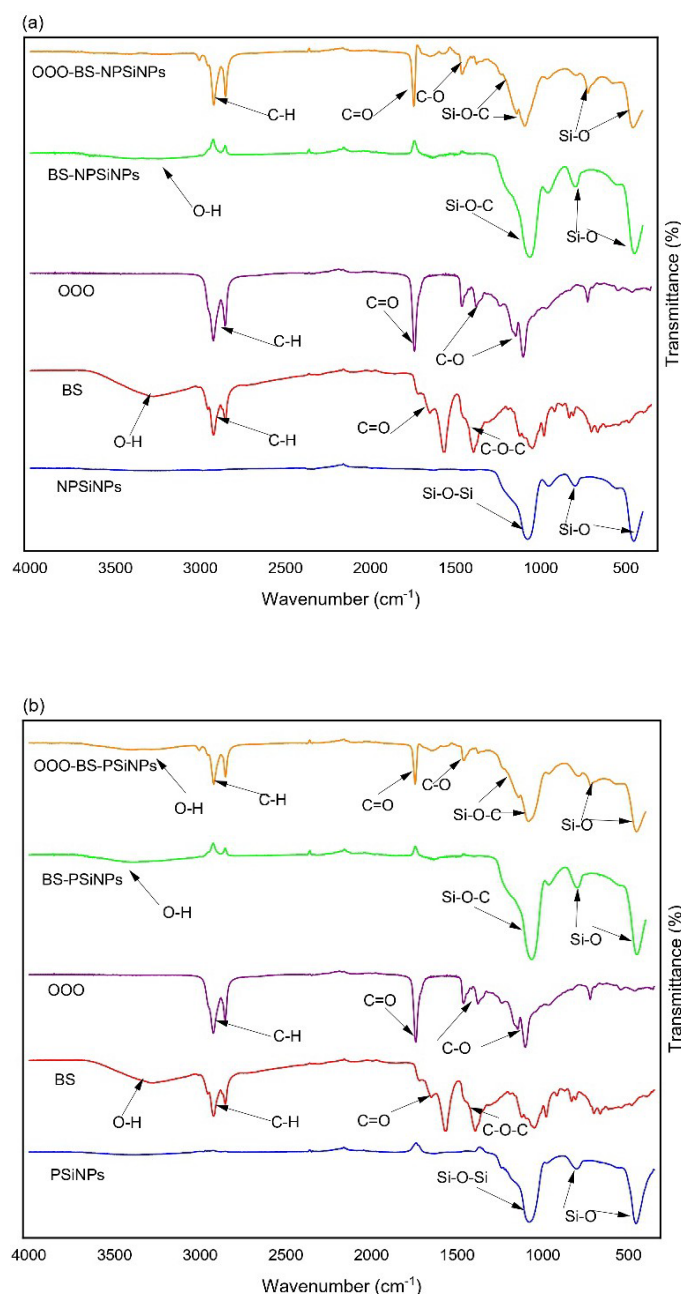


Fig. 3. FT-IR spectra for (a) NPSiNPs and (b) PSiNPs.
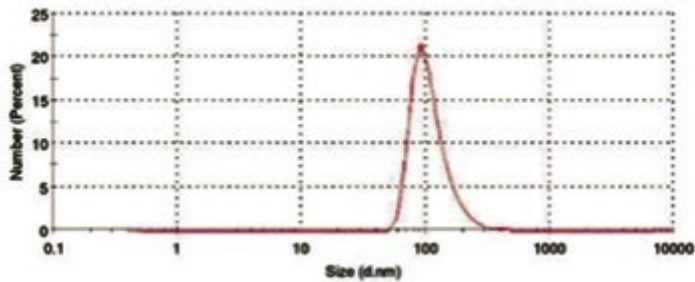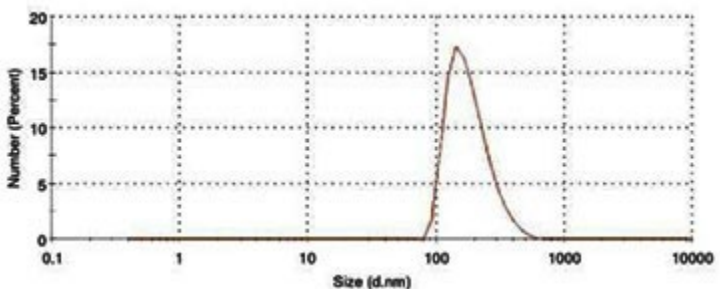
### 3.2.2. Size and particles dispersibility

DLS was used to analyze the polydispersibility index (PDI) and the size distribution of both silica nanoparticles. From Table 1, NPSiNPs exhibit a peak diameter of 109.9 nm with a PDI of 0.137, indicating a monodisperse system with uniform particle size. After coating with BS, the size of the BS-NPSiNPs increases to 156.7 nm, reflecting the addition of the coating layer while maintaining a narrow size distribution (PDI of 0.153), indicating stable particle formation. However, when OOO is introduced, the size decreases to 137.4 nm, and the PDI increases to 0.348, indicating a broader size distribution for OOO-BS-NPSiNPs. The increase in PDI suggests that the OOO affects the uniformity of the particles, likely due to interaction with the biosurfactant and silica surface, leading to a more polydisperse system.

PSiNPs are larger at 185.2 nm compared to NPSiNPs, with a slightly higher PDI of 0.218, indicating a more polydisperse system due to their porous structure, which aligns with previous observations regarding aggregation behavior. After coating with BS, the size of BS-PSiNPs decreases to 158.1 nm, suggesting that the BS fills the pores and interacts with the surface, resulting in a slight size reduction. The PDI remains nearly unchanged at 0.228, indicating a stable and uniform coating process. In contrast, the particle size of OOO-BS-PSiNPs further decreases to 148.4 nm, but the PDI increases significantly to 0.597, indicating a highly polydisperse system.
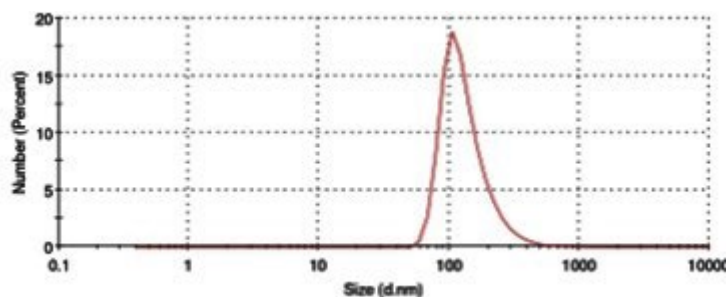
Table 1: Size distribution and PDI value of nanofluids suspension

| Sample | Size Distribution Graph | Peak (d.nm) | PDI |
|---|---|---|---|
| NPSiNPs |  | 109.9 | 0.137 |
| BS-NPSiNPs |  | 156.7 | 0.153 |

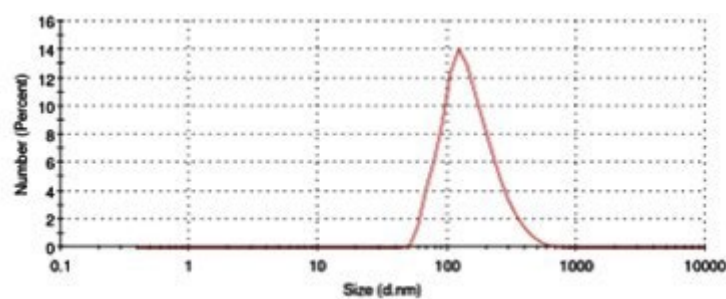| OOO-BS-NPSiNPs | | 137.4 | 0.348 |



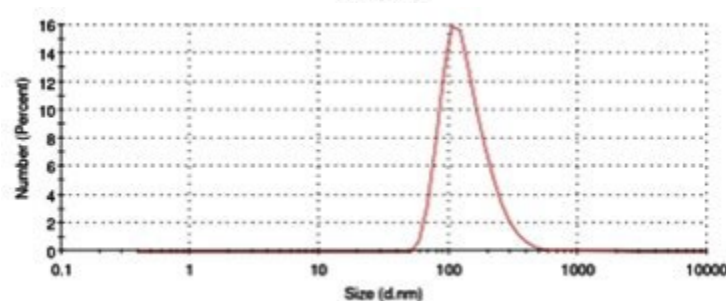| PSiNPs | | 185.2 | 0.218 |



| BS-PSiNPs | | 158.1 | 0.228 |



| OOO-BS-PSiNPs | | 148.4 | 0.597 |
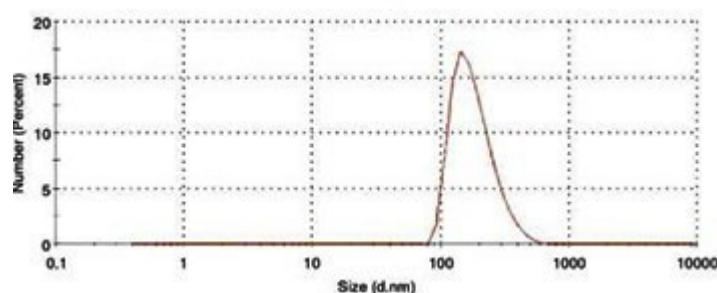


## 3.3. Stability test of SiNP

Visual inspection and UV-vis absorbance spectra were used to assess the stability of SiNPs loaded with OOO. A gradual decrease in absorbance over three days indicated a tendency for nanoparticle aggregation and settling. Initially, OOO-BS-PSiNPs showed good dispersion and high absorbance on Day 1. However, stability declined significantly, with approximately 50% of the particles settling by Day 3. In contrast, OOO-BS-NPSiNPs exhibited enhanced stability, maintaining higher absorbance through Day 3, with only a 19% reduction in suspension, indicating improved long-term stability. This reflects a stronger resistance to aggregation and settling, essential for maintaining suspended nanoparticles over time [22]. The rapid decline in absorbance for OOO-BS-PSiNPs suggests that their porous structure may contribute to interactions promoting faster aggregation or settling. The high surface area and rough morphology of porous nanoparticles increase intermolecular forces, leading to enhanced particle-particle interactions, which may

facilitate aggregation [23]. In contrast, non-porous nanoparticles typically exhibit better stability due to their lower surface area and reduced particle-particle interactions [24]. This behavior is common in nanoparticle suspensions, where interactions between particles or with the medium play a key role in stability and dispersion [25]. Thus, NPSiNPs demonstrated better long-term stability, making them more suitable for applications such as cosmetics and medicine, which require prolonged suspension and uniform dispersion of nanoparticles.

The stability test was conducted on both NPSiNPs and PSiNPs to visually assess the sedimentation and aggregation of OOO-BS-SiNPs in aqueous media. The study was carried out in 24 hrs. As detailed in Table 2, initially both NPSiNPs and PSiNPs remained uniformly dispersed at their initial concentrations. However, after 24 hrs, signs of sedimentation began to appear. To conclude, the stability test indicates that while NPSiNPs and PSiNPs initially maintain dispersion, sedimentation becomes apparent after 24 hrs. Despite this, a fraction of the silica nanoparticles continues to be dispersed in deionized water, suggesting partial stability in aqueous environments. In contrast, it was obvious that both OOO-BS-NPSiNPs and OOO-BS-PsiNPs remained in the suspension after 24 hrs which supports the results in Table 1 and Fig. 4. This finding suggests that the suspension of the nanofluids enhanced with the combination of OOO, BS and the SiNPs compared to SiNPs alone or BS and SiNPs.
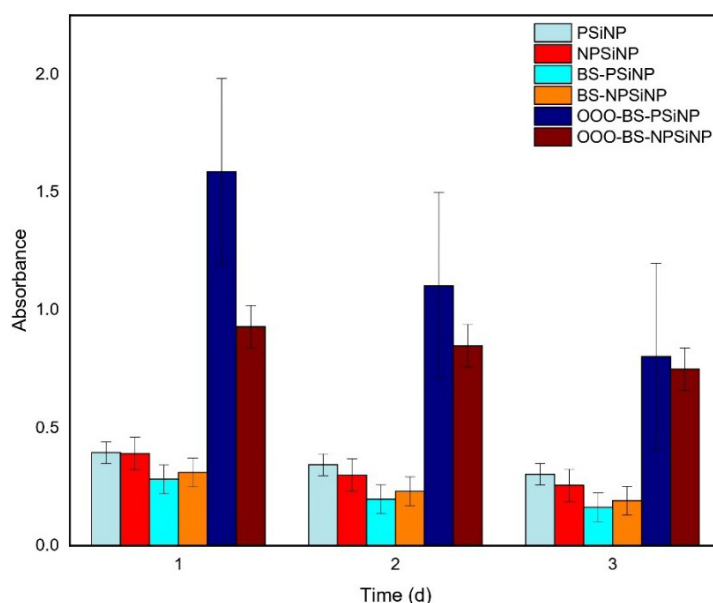


Fig. 4. UV Vis absorption of the stability of the nanofluids in aqueous solution with time.

Table 2: Visual observation of nanofluid suspensions at 24 hrs.

| Samples | 0hr | 24hrs |
| --- | --- | --- |
| **NPSiNPs** | | |
| **BS-NPSiNPs** | | |
| **OOO-BS-NPSiNPs** | | |
| **PSiNPs** | | |
| **BS-PSiNPs** | | |

OOO-BS-PSiNPs

## 4. CONCLUSION

This study demonstrated that silica nanoparticles can effectively immobilize OOO, addressing key challenges in its wettability and stability in aqueous solutions. The findings underscore the impact of nanoparticle structure and the role of rhamnolipid biosurfactants in enhancing the bioavailability and prolonged stability of OOO. It was found that NPSiNPs exhibited higher OOO loading capacity and stability in suspension than PSiNPs. This study is significant for fields such as wound healing and antimicrobial therapy, where the antibacterial properties of OOO-BS-SiNPs can be effectively utilized to enhance therapeutic outcomes. However, challenges such as sedimentation and aggregation tendencies in aqueous media should be addressed in future investigations. Furthermore, investigating the controlled release kinetics of OOO from SiNPs and performing biocompatibility assessments are essential for advancing their potential applications in drug delivery and environmental remediation. These results contribute to advancements in therapeutic applications for OVO and lay a strong foundation for further research in nanoparticle-based delivery systems using OVO. They also provide a foundation for future research in this field.

## ACKNOWLEDGEMENT

## REFERENCES

[1] Yalçin TE, Takka S. (2020) Development and characterization of camphor-loaded ozonated olive oil nanoemulsions. Journal of Research in Pharmacy, 24(6):935–942.

[2] Amri Z, Ben Hamida S, Dbeibia A, Ghorbel A, Mahdhi A, Znati M, Ambat I, Haapaniemi E, Sillanpää M, Hammami M. (2020) Physico-chemical Characterization and Antibacterial Activity of Ozonated Pomegranate Seeds Oil. Ozone: Science and Engineering, 42(6): 531–538.

[3] Guerra-Blanco P, Chairez I, Poznyak T, Brito-Arias M. (2021) Kinetic Analysis of Ozonation Degree Effect on the Physicochemical Properties of Ozonated Vegetable Oils. Ozone: Science and Engineering, 43(6):546–561.

[4] Silva V, Peirone C, Amaral JS, Capita R, Alonso-Calleja C, Marques-Magallanes JA, Martins Â, Carvalho Á, Maltez L, Pereira JE, Capelo JL, Igrejas G, Poeta P. (2020) High efficacy of ozonated oils on the removal of biofilms produced by methicillin-resistant staphylococcus aureus (MRSA) from infected diabetic foot ulcers. Molecules, 25(16).

[5] Radzimierska-Kazmierczak M, Smigielski K, Sikora M, Nowak A, Plucinska A, Kunicka-

Styczynska A, Czarnecka-Chrebelska KH. (2021) Olive oil with ozone-modified properties and its application. Molecules, 26(11).

[6]  Aguirre-Ramírez M, Silva-Jiménez H, Banat IM, Díaz De Rienzo MA. (2021) Surfactants: physicochemical interactions with biological macromolecules. In Biotechnology Letters (Vol. 43, Issue 3, pp. 523–535). Springer Science and Business Media B.V.

[7]  Fahmy SA, Ramzy A, Sawy AM, Nabil M, Gad MZ, El-Shazly M, Aboul-Soud MAM, Azzazy HMES. (2022) Ozonated Olive Oil: Enhanced Cutaneous Delivery via Niosomal Nanovesicles for Melanoma Treatment. Antioxidants, 11(7).

[8]  Ugazio E, Tullio V, Binello A, Tagliapietra S, Dosio F. (2020) Ozonated oils as antimicrobial systems in topical applications. Their characterization, current applications, and advances in improved delivery techniques. In Molecules (Vol. 25, Issue 2). MDPI AG.

[9]  Nayl AA, Abd-Elhamid AI, Aly AA, Bräse S. (2022) Recent progress in the applications of silica-based nanoparticles. In RSC Advances (Vol. 12, Issue 22, pp. 13706–13726). Royal Society of Chemistry.

[10]  Mehmood Y, Haroon Khalid S. (2019) Facile synthesis of mesoporous silica nanoparticles using modified sol-gel method: Optimization and in vitro cytotoxicity studies. In Article in Pakistan Journal of Pharmaceutical Sciences (Vol. 40).

[11]  Moulydia F, Salsabila N, Dewi RK, Nirmala A, Bismo, S. (2018) Burn drug made from ozonated vegetable oil mixture with white tumeric and cassava leaves extract. MATEC Web of Conferences, 154.

[12]  Bukke SPN, Venkatesh C, Bandenahalli Rajanna S, Saraswathi TS, Kusuma PK, Goruntla N, Balasuramanyam N, Munishamireddy S. (2024) Solid lipid nanocarriers for drug delivery: design innovations and characterization strategies—a comprehensive review. In Discover Applied Sciences (Vol. 6, Issue 6). Springer Nature.

[13]  Pinzon NM, Ju LK. (2009) Analysis of rhamnolipid biosurfactants by methylene blue complexation. Applied Microbiology and Biotechnology, 82(5):975–981.

[14]  Xu R, et al. (2020). Application of silica nanoparticles for enhanced oil recovery: A review of recent advances. Journal of Petroleum Science and Engineering, 187, 106870.

[15]  Wang J, Shah ZH, Zhang S, Lu R. (2014) Silica-based nanocomposites via reverse microemulsions: Classifications, preparations, and applications. In Nanoscale (Vol. 6, Issue 9, pp. 4418–4437).

[16]  Wang W, Wang P, Tang X, Elzatahry AA, Wang S, Al-Dahyan D, Zhao M, Yao C, Hung C. Te Zhu X, Zhao T, Li X, Zhang F, Zhao D. (2017) Facile Synthesis of Uniform Virus-like Mesoporous Silica Nanoparticles for Enhanced Cellular Internalization. ACS Central Science, 3(8): 839–846.

[17]  Rosdi, N.A (2022) Ozonation of Vegetable oils and study on its Physicochemical and Biological Characteristic [Final year project thesis, International Islamic University Malaysia]

[18]  Khouchaf L, Boulahya K, Das PP, Nicolopoulos S, Kis VK, Lábár JL. (2020) Study of the microstructure of amorphous silica nanostructures using high-resolution electron microscopy, electron energy loss spectroscopy, X-ray powder diffraction, and electron pair distribution function. Materials, 13(19):1–14.

[19]  Deshmukh P, Bhatt J, Peshwe D, Pathak S. (2012) Determination of silica activity index and XRD, SEM and EDS studies of amorphous SiO 2 extracted from rice Husk Ash. Transactions of the Indian Institute of Metals, 65(1):63–70.

[20]  Zhou Y, Wu X, Zhong X, Sun W, Pu H, Zhao JX. (2019) Surfactant-Augmented Functional Silica Nanoparticle Based Nanofluid for Enhanced Oil Recovery at High Temperature and Salinity. ACS Applied Materials and Interfaces, 11(49):45763–45775.

[21]  Rahman IA, Vejayakumaran P, Sipaut CS, Ismail J, Chee CK. (2009) Size-dependent physicochemical and optical properties of silica nanoparticles. Materials Chemistry and Physics, 114(1):328–332.

[22]  Xu Z, Tang Q, Hong A, Li L. (2022) Aggregation, Sedimentation and Dissolution of Cu(OH)2-Nanorods-Based Nanopesticide in Soil Solutions. Nanomaterials, 12(21).

[23]  Wu A, Yang C, Zhao X, Wang J, Liang W, Wang X, Zhou L, Teng M, Hou G, Niu L, Tang

Z, Wu F. (2024) Heteroaggregation and sedimentation of natural goethite and artificial $Fe_3O_4$ nanoparticles with polystyrene nanoplastics in water. Carbon Research, 3(1).

[24] Bidyarani N, Srivastav, AK, Gupta SK, Kumar U. (2020) Synthesis and physicochemical characterization of rhamnolipid-stabilized carvacrol-loaded zein nanoparticles for antimicrobial application supported by molecular docking. Journal of Nanoparticle Research, 22(10).

[25] Lavagna E, Barnoud J, Rossi G, Monticelli L. (2020) Size-dependent aggregation of hydrophobic nanoparticles in lipid membranes. Nanoscale, 12(17):9452–9461.